

Multiplex visibility graphs to investigate recurrent neural networks dynamics

Filippo Maria Bianchi^{1,*}, Lorenzo Livi^{2,3,4}, Cesare Alippi^{2,3}, and Robert Jenssen¹

¹Machine Learning Group, Dept. of Physics and Technology, University of Tromsø, Hansine Hansens veg 18, 9019 Tromsø, Norway

²Dept. of Computer Science, College of Engineering, Mathematics and Physical Sciences, University of Exeter, Exeter EX4 4QF, UK

³Dept. of Electronics, Information, and Bioengineering, Politecnico di Milano, Piazza Leonardo da Vinci 32, 20133 Milano, Italy

⁴Faculty of Informatics, Università della Svizzera Italiana, Via Giuseppe Buffi 13, 6904 Lugano, Switzerland

*filippo.m.bianchi@uit.no

ABSTRACT

A recurrent neural network (RNN) is a universal approximator of dynamical systems, whose performance often depends on sensitive hyperparameters. Tuning of such hyperparameters may be difficult and, typically, based on a trial-and-error approach. In this work, we adopt a graph-based framework to interpret and characterize the internal RNN dynamics. Through this insight, we are able to design a principled unsupervised method to derive configurations with maximized performances, in terms of prediction error and memory capacity. In particular, we propose to model time series of neurons activations with the recently introduced horizontal visibility graphs, whose topological properties reflect important dynamical features of the underlying dynamic system. Successively, each graph becomes a layer of a larger structure, called multiplex. We show that topological properties of such a multiplex reflect important features of RNN dynamics and are used to guide the tuning procedure. To validate the proposed method, we consider a class of RNNs called echo state networks. We perform experiments and discuss results on several benchmarks and real-world dataset of call data records.

Introduction

Research on complex dynamical systems is focusing more and more on networks characterized by time-variant properties¹, which can be related to the topology and/or features associated with vertices and edges (e.g., the states of networked dynamic systems, such as those emerging from cyber-physical systems and the Internet of Things). Of particular interest are those systems that also perform a computation when driven by an external input signal. An example are the RNNs^{2,3}, which are gaining increasing attention in neuroscience due to their biological plausibility⁴. RNNs are universal approximators of Lebesgue measurable dynamical systems⁵, with the capability to store the history of input signals and perform inference^{6,7}. A RNN depends on several hyperparameters, whose tuning can highly affect the performance on a given task. The recurrent nature of RNNs complicates training and hamper the interpretability of the internal dynamics⁸. This poses constraints on the applicability of the model, which is usually treated as a blackbox and its hyperparameters are tuned by cross-validation. However, cross-validation comes with shortcomings. Being a supervised form of model selection, it requires to evaluate the performance on a validation set. This might be an important limitation in real-life applications, where the amount of data is scarce and supervised information not always available. Moreover, the model has to be re-trained for each hyperparameter configuration; this is an issue whenever the learning procedure is computationally demanding.

Different unsupervised methods for tuning RNN hyperparameters have been proposed in the literature^{9–11}. Of particular interest are those aiming to identify the so-called *edge of criticality* (e.g., see^{12–14} and references therein), namely the set of hyperparameters for which a RNN shows a dynamical behavior lying in-between order and chaos. On such configurations, RNNs usually achieve the best performance in terms of prediction accuracy and memory capacity, which are the quantities generally monitored by model selection techniques based on cross-validation. Notably, for tasks where the RNN receives the same input sequence, configurations that bring the RNN to the edge of criticality are identical and can be identified just once. Contrarily to the blackbox approach proper of cross-validation methods, many of these unsupervised approaches offer an insight of the RNN functioning, providing an interpretable model of the system dynamics. A RNN is driven by inputs and assumptions on their nature are necessary to investigate dynamical properties. Alternatively, one can follow a data-driven approach and observe the dynamics of the recurrent layer neurons through time. These approaches are often based on statistical tools, which require samples to be independent and identically distributed (i.i.d.). However, in neuron activations the latter

requirement does not hold when RNNs are driven by a non-stationarity input signal¹⁵. Independence, instead, is violated by the temporal correlations introduced by the recurrent connections. Additionally, the unsupervised tuning seldom achieves same level of accuracy of the supervised counterpart.

With this work, we propose an new unsupervised approach to (i) identify the edge of criticality by analyzing dynamics of neuron activations through a graph-based approach and (ii) tune the hyperparameters accordingly. In our framework, temporal relations in time series of activations are converted into topological connections of a graph. This is essential to overcome the limitations of the i.i.d. requirement in statistical methods. Additionally, we provide evidence that the proposed method is able to achieve performance comparable with supervised techniques, thus resolving the shortcomings of existing unsupervised approaches. A key aspect in our proposed framework is to analyze the activity of neurons in the recurrent layer by mapping the multivariate time series of activations into a multiplex. A multiplex network^{16–20} is a special type of multilayer (complex) network, characterized by a specific structure, where vertices are replicated through the layers and are connected across layers only with their replicas. The topology (i.e., the edges) of the graphs in each layer can be different. Here, we use the multiplex visibility graph, recently proposed in²¹, whose layers consists of a particular class of graph called horizontal visibility graph (HVG)^{22,23}. HVGs are planar graphs constructed from real-valued time series, whose values have one-to-one correspondence with the vertices. Many important properties have been recently studied, which link the structure of HVGs with features of the dynamic system (e.g., chaos) underlying the analyzed time series^{24–27}.

The key novelty of this paper is to characterize RNN dynamics through structural characteristics of the multiplex. Specifically, we represent the instantaneous state of a RNN through a set of vertex properties of the multiplex (e.g., degree, clustering coefficient). Edges in HVGs might cover a relevant time frame (contained within the longest period of the signal), while they are still local in terms of topology. Accordingly, the RNN instantaneous state can be characterized also by information that are non-local in time. To optimally tune the hyperparameters, we follow the hypothesis that RNN computational capability is high if its internal dynamical patterns are sufficiently rich¹³. Accordingly, we look for configurations yielding neuron activations that are as diverse as possible in order to achieve maximal prediction accuracy. Within the proposed framework, we show how the heterogeneity in neuron dynamics can be effectively captured by the entropy of vertex properties of the multiplex. To quantify the amount of memory in the RNN associated with a given configuration, we check the existence of neuron activations that are “similar” to different delayed versions of the input. In fact, memory in RNNs depends on the ability to recreate past versions of the input, whose dynamics information must be kept in some neuron activations. We describe dynamics of delayed inputs and of neuron activations through unsupervised graph-based measures. Then, by evaluating the agreement between such measurements, we characterize the memory capacity in RNNs with a high degree of accuracy, compatible to the outcome of a supervised method.

Although our framework is applicable to any RNN, in the following we focus on echo state network (ESN) models^{28–30}.

Methods

Echo state networks

A standard ESN architecture consists of a large recurrent layer of non-linear units connected by randomly generated weights and a linear, memory-less readout layer that can be trained with a regularized least-square optimization²⁸. The recurrent layer acts as a non-linear kernel³¹, mapping the input to a high-dimensional space. The equations describing the ESN state-update and output are, respectively, defined as

$$\mathbf{h}[t] = f(\mathbf{W}_r^r \mathbf{h}[t-1] + \mathbf{W}_i^r \mathbf{u}[t] + \mathbf{W}_o^r \mathbf{y}[t-1]), \quad (1)$$

$$\mathbf{y}[t] = \mathbf{W}_i^o \mathbf{u}[t] + \mathbf{W}_r^o \mathbf{h}[t]. \quad (2)$$

The reservoir contains N_r neurons whose transfer/activation function $f(\cdot)$ is typically implemented by a hyperbolic tangent. At time instant t , the ESN is driven by the input signal $\mathbf{u}[t] \in \mathbb{R}^{N_i}$ and it produces the output $\mathbf{y}[t] \in \mathbb{R}^{N_o}$, being N_i and N_o the dimensionality of input and output, respectively. The vector $\mathbf{h}[t] \in \mathbb{R}^{N_r}$ describes the ESN (instantaneous) state. The weight matrices $\mathbf{W}_r^r \in \mathbb{R}^{N_r \times N_r}$ (reservoir connections), $\mathbf{W}_i^r \in \mathbb{R}^{N_i \times N_r}$ (input-to-reservoir), and $\mathbf{W}_o^r \in \mathbb{R}^{N_o \times N_r}$ (output-to-reservoir feedback) contain real values in the $[-1, 1]$ interval, sampled from a uniform distribution. Weights in \mathbf{W}_i^o and \mathbf{W}_r^o , instead, are learned (typically by means of regularized least-square algorithm) according to the task at hand.

Once given, the designer can control \mathbf{W}_r^r , \mathbf{W}_i^r , and \mathbf{W}_o^r only by using suitable scaling coefficients. \mathbf{W}_o^r is scaled through a multiplicative constant ω_o . In this study, output feedback is removed by setting $\omega_o = 0$. Hence, the resulting state-update equation becomes

$$\mathbf{h}[t] = f(\mathbf{W}_r^r \mathbf{h}[t-1] + \mathbf{W}_i^r \mathbf{u}[t]), \quad (3)$$

while the output (2) remains unchanged. Input weights in \mathbf{W}_i^r are controlled by a scalar parameter ω_i that determines the amount of non-linearity (saturation) introduced by neurons. The spectral radius ρ of \mathbf{W}_r^r is known to influence both stability and

computational capability of the ESN. Asymptotic stability is guaranteed by the so-called echo state property, which requires the reservoir to exhibit a fading memory of past inputs³².

Both ρ and ω_i are typically set with a cross-validation procedure to find the best configuration for the task at hand, yet some unsupervised approaches have been proposed to tune these quantities. In particular, the degree of predictability of the ESN can be assessed from the Maximal Local Lyapunov Exponent (MLLE), which measures the separation rate in phase space of trajectories with similar initial states. In autonomous systems, transition to chaos is identified when $\text{MLLE} = 0$. Here, we are interested in a quantity which can be compared with prediction accuracy and memory capacity. However, MLLE increases monotonically with the degree of chaoticity of the ESN. On the other hand, the minimal singular value (in average, over time) of the reservoir Jacobian, denoted as λ , can accurately detect the onset of criticality in dynamic systems and is well correlated with ESN performance¹⁰. In fact, λ is unimodal and in correspondence of its maximum, the dynamical system is far from singularity, it has many degrees of freedom, a good excitability, and it separates well the input signals in phase space. Assuming input zero in Eq. 3, the Jacobian matrix of the reservoir at time t is given by $\mathbf{J}_t = \text{diag}(1 - (\mathbf{h}_1[t])^2, 1 - (\mathbf{h}_2[t])^2, \dots, 1 - (\mathbf{h}_{N_r}[t])^2) \mathbf{W}_r^T$, $\text{diag}(\cdot)$ returns a diagonal matrix.

Horizontal visibility graph and multiplex network

The HVG²² associated to an univariate time series $\{\mathbf{x}[t]\}_{t=1}^{t_{\max}}$, is constructed by assigning a vertex v_t to each datum $\mathbf{x}[t]$ and is represented by a binary adjacency matrix \mathbf{A} . Two vertices v_i and v_j , $i \neq j$, are connected by an edge ($\mathbf{A}[i, j] = 1$) if the corresponding data fulfill the criterion $\mathbf{x}[t_i], \mathbf{x}[t_j] > \mathbf{x}[t_p], \forall t_i < t_p < t_j$. In a multivariate scenario, the data stream is composed of N_r different time series $\{\mathbf{x}_l\}_{l=1}^{N_r}$, of equal length t_{\max} . As proposed in²¹, the multivariate time series is mapped into a multiplex visibility graph \mathcal{M} with N_r layers. The l th multiplex layer is defined by the HVG G_l constructed from \mathbf{x}_l . In the multiplex, a vertex is replicated on all layers and such replicas are linked by inter-layer connections, while intra-layer connections might change in each layer. From now on, with $\mathbf{v}_l[t]$ we refer to the vertex of G_l in layer l associated to time interval t .

In this paper we introduce a weighted HVG (wHVG), with edges defined as $\mathbf{A}[i, j] = 1/\sqrt{(j-i)^2 + (\mathbf{x}[i] - \mathbf{x}[j])^2}$. Note that since self-loops are forbidden in HVGs, edge weights are always well-defined. This variant captures additional information, since it accounts for both temporal and amplitude differences in the connected data. In the experimental section, we provide examples of RNN dynamics that are better characterized by wHVGs than by the original binary formulation. Algorithm 1 delivers the pseudo-code for constructing a HVG (wHVG). To evaluate the complexity of this algorithm, we first consider the $\mathcal{O}(t_{\max}^2)$ worst case, which occurs when the time-series \mathbf{x} is monotonically decreasing. In the best case scenario, the values in \mathbf{x} increase monotonically and the time complexity becomes $\mathcal{O}(t_{\max})$.

Algorithm 1 Algorithm for constructing a (weighted) HVG.

Input: A time series $\{\mathbf{x}[t]\}_{t=1}^{t_{\max}}$
Output: Adjacency matrix \mathbf{A} of (weighted) HVG

```

1: for  $i = 1, \dots, t_{\max} - 1$  do
2:   Set  $j = i + 1$ ,  $\max = -\infty$ ,  $\text{stop} = \text{false}$ ,  $\text{count} = 0$ 
3:   while  $\text{stop}$  is false AND  $j \leq n$  do
4:      $\text{count} = \text{count} + 1$ 
5:     if  $\mathbf{x}[j] > \max$  then
6:       If unweighted,  $\mathbf{A}[i, j] = 1$ , otherwise,  $\mathbf{A}[i, j] = 1/\sqrt{(j-i)^2 + (\mathbf{x}[i] - \mathbf{x}[j])^2}$ 
7:        $\max = \mathbf{x}[j]$ 
8:       if  $\max > \mathbf{x}[i]$  then
9:          $\text{stop} = \text{true}$ 
10:      end if
11:    end if
12:     $j = j + 1$ 
13:  end while
14: end for

```

Vertex properties and heterogeneity measure

Let us consider an ESN with a reservoir of size N_r , driven by an input of length t_{\max} . According to Eq. 3, the ESN generates N_r time series $\{\mathbf{h}_1[t]\}_{t=1}^{t_{\max}}, \dots, \{\mathbf{h}_{N_r}[t]\}_{t=1}^{t_{\max}}$, relative to neuron activations. The multivariate time series $\{\mathbf{h}_l\}_{l=1}^{N_r}$ is represented here by a multiplex \mathcal{M} . Indexes of the vertices on each layer l of \mathcal{M} are one-to-one associated with the time index of the original time series. Hence, the ESN state $\{\mathbf{h}_l[t]\}_{l=1}^{N_r}$ at time t is represented by the vertices $\{\mathbf{v}_l[t]\}_{l=1}^{N_r}$ and, more interestingly, by their vertex properties $\Phi^*[t] = \{\phi^*(\mathbf{v}_l[t])\}_{l=1}^{N_r}$. In Tab. 1 we introduce four vertex properties: degree, clustering coefficient³³, betweenness and closeness centrality³⁴. Therefore, to quantify the richness/diversity of ESN internal dynamics we evaluate the heterogeneity of these properties over time. Heterogeneity is calculated by elaborating over the entropy of the vertex properties distribution. This allows to account also higher-order moments. Heterogeneity is computed as follows:

1. At each time t , evaluate the vertex properties $\Phi^*[t] = \{\phi^*(\mathbf{v}_l[t])\}_{l=1}^{N_r}$ using one of the measures listed in Tab. 1.

2. Approximate distribution $p(\Phi^*[t])$ using a histogram with b bins.
3. Compute instantaneous entropy: $H_t = H(p(\Phi^*[t]))$, where $H(\cdot)$ is the Shannon entropy.
4. Define heterogeneity as average entropy over time instants: $\bar{H} = \frac{1}{t_{\max}} \sum_{t=1}^{t_{\max}} H_t$.

Table 1. Vertex characteristics used to generate different instances of the vertex property vector ϕ_t .

Vertex degree	$\phi^{\text{DG}}(v) = \sum_i \mathbf{A}[i, v]$	Number of edges incident to a vertex v .
Clustering coefficient	$\phi^{\text{CL}}(v) = \frac{\sum_{i \in \mathcal{C}_v} \sum_{j \in \mathcal{C}_v} \mathbf{A}[i, j]}{ \mathcal{C}_v (\mathcal{C}_v - 1)}$	Clustering coefficient of a vertex v defined in ³⁵ , applicable to both weighted and binary graphs. Originally, $\mathcal{C}_v = \{i \mathbf{A}[i, v] \neq 0 \vee \mathbf{A}[v, i] \neq 0\}$, but we used a slight variation by considering the set $\mathcal{C}_v^* = \{v \cup \mathcal{C}_v\}$ that includes also the vertex v (and its edges) in the set of vertices to evaluate.
Betweenness Centrality	$\phi^{\text{BC}}(v) = \sum_{i \neq v \neq j} \frac{\sigma_{ij}(v)}{\sigma_{ij}}$	Measures the centrality of a vertex v . σ_{ij} is total number of shortest paths from i to j and $\sigma_{ij}(v)$ denotes the number of shortest paths passing through v .
Closeness centrality	$\phi^{\text{CC}}(v) = \sum_{v \neq i} 2^{- \sigma(i, v) }$	Total distance of a vertex v from all other vertices in the graph. $ \sigma(i, v) $ denotes the length of the shortest path between i and v .

Memory measures

Memory capacity (MC)²⁸ is a supervised measure, used to describe the capability of ESN to remember previous input values. To evaluate MC the reservoir is kept fixed, while several readout layers are trained to reproduce past versions of the same input at different time lags $\tau_{L_1}, \dots, \tau_{L_{\max}}$. The expression reads

$$\text{MC} = \sum_{\tau_L} \frac{\text{cov}^2(\mathbf{x}[t - \tau_L], \mathbf{y}[t])}{\text{var}(\mathbf{x}[t - \tau_L]) \text{var}(\mathbf{y}[t])}. \quad (4)$$

In the following, we introduce unsupervised measures that quantify RNN memory. Given G_l , the HVG representing the l th layer of the multiplex, $\Phi_l^{\text{DG}} = \{\phi^{\text{DG}}(\mathbf{v}_l[t])\}_{t=1}^{t_{\max}}$ is the sequence of its vertex degrees ordered according to the time index (not to be confused with $\Phi^{\text{DG}}[t] = \{\phi^{\text{DG}}(\mathbf{v}_l[t])\}_{l=1}^{N_r}$, the degree sequence of vertices relative to time t across the different layers). With $G_{\mathbf{x}}$, instead, we refer to the HVG constructed over the input \mathbf{x} . Accordingly, $\Phi_{\mathbf{x}}^{\text{DG}}$ is the vector of its vertex degrees.

First, we define a measure of maximum agreement between $\Phi_{\mathbf{x}}^{\text{DG}}$ and each sequence Φ_l^{DG} as $\delta^{\text{DG}} = \max_l \kappa^*(\Phi_{\mathbf{x}}^{\text{DG}}, \Phi_l^{\text{DG}})$. Here, $\kappa^*(\cdot, \cdot)$ is a similarity measure between sequences: we consider Pearson correlation $\kappa^{\text{PC}}(\cdot, \cdot)$, Spearman correlation $\kappa^{\text{SC}}(\cdot, \cdot)$, and mutual information $\kappa^{\text{MI}}(\cdot, \cdot)$.

A second measure of agreement is defined on the adjacency matrix $\mathbf{Q}_l = \mathbf{A}_{\mathbf{x}} \wedge \mathbf{A}_l$, where $\mathbf{Q}_l[i, j] = 1$ if $\mathbf{A}_{\mathbf{x}}[i, j] = 1 \wedge \mathbf{A}_l[i, j]$, $\mathbf{Q}_l[i, j] = 0$ otherwise. Agreement is then computed as the highest number of edges among all the possible intersection graphs, $\delta^{\text{AND}} = \max_l |\mathbf{Q}_l|$, where $|\cdot|$ counts the number of ones in the adjacency matrix.

Finally, one could conceive a measure that directly considers the agreement between input \mathbf{x} and neuron activations \mathbf{h}_l , $\delta^{\text{TS}} = \max_l \kappa^*(\mathbf{x}, \mathbf{h}_l)$. Now, $\kappa^*(\cdot, \cdot)$ is evaluated on the time series rather than on the sequences of vertex degrees.

Other multiplex complexity measures

In²¹, two measures are proposed to characterize the dynamics of a system observed through a multivariate time series and represented as a multiplex HVG. We take them into account, to evaluate whether they are useful to identify the edge of criticality. The Average Edge Overlap (AEO) computes the expected number of layers of the multiplex on which an edge is present. It is defined, for binary HVGs, as

$$\text{AEO} = \frac{\sum_i \sum_{j>i} \sum_l \mathbf{A}_l[i, j]}{N_r \sum_i \sum_{j>i} (1 - \delta_{0, \sum_l \mathbf{A}_l[i, j]})},$$

where $\mathbf{A}_l[i, j]$ is 1 if vertices i and j are connected in layer l . The second measure is the Interlayer Mutual Information (IMI), which quantifies the correlations between the degree distributions of two different layers l_i and l_j . It is defined, for binary HVGs, as

$$\text{IMI}(l_i, l_j) = \sum_{k_{l_i}} \sum_{k_{l_j}} p(k_{l_i}, k_{l_j}) \log \left(\frac{p(k_{l_i}, k_{l_j})}{p(k_{l_i}) p(k_{l_j})} \right),$$

where $p(k_{l_i}, k_{l_j})$ is the joint probability to find a vertex with degree k_{l_i} in layer l_i and degree k_{l_j} in layer l_j , respectively. In the experiments, we use the average IMI between all pairs of multiplex layers.

Results

In this section, we evaluate the effectiveness of the proposed unsupervised multiplex measures to characterize neuron activations and hence to quantify the computational capability of ESNs. Notably, we provide an unsupervised method to identify the edge of criticality, which is the set of hyperparameter configurations where the ESN achieves highest performance, in terms of prediction accuracy and memory capacity. We stress that, although we frame our contribution in terms of ESN, our results are general and applicable to virtually each RNN. In the first experiment we compare, for different hyperparameter configurations, the correlation of the prediction accuracy achieved on several tasks with the heterogeneity of vertex properties in the multiplex. Accordingly, we show that the locations in parameter space where the heterogeneity is maximized correspond to ESN configurations where the prediction accuracy is maximal as well. In a second experiment, we provide evidence of how unsupervised graph-based measures can be used to identify configurations yielding ESNs with largest memory capacity.

Test on prediction accuracy

In order to find configurations where prediction accuracy is maximized, we look for hyperparameters yielding neuron activations that are as heterogeneous as possible. In fact, it is well-known that RNNs (and then also ESNs) are effective if their internal dynamical patterns are sufficiently rich. In the literature, this is usually expressed in terms of entropy, diversity of connection weights or rank of the matrix of neuron activations^{13,30,36}.

Fig. 1 provides a schematic illustration of the concept herein discussed. For a RNN driven by a sinusoid, we depict the neuron activations and the corresponding HVGs. We select a time step and we show the correspondence between the values in each time series (marked by a black square in the picture) and the vertices in the associated HVGs. When the RNN is

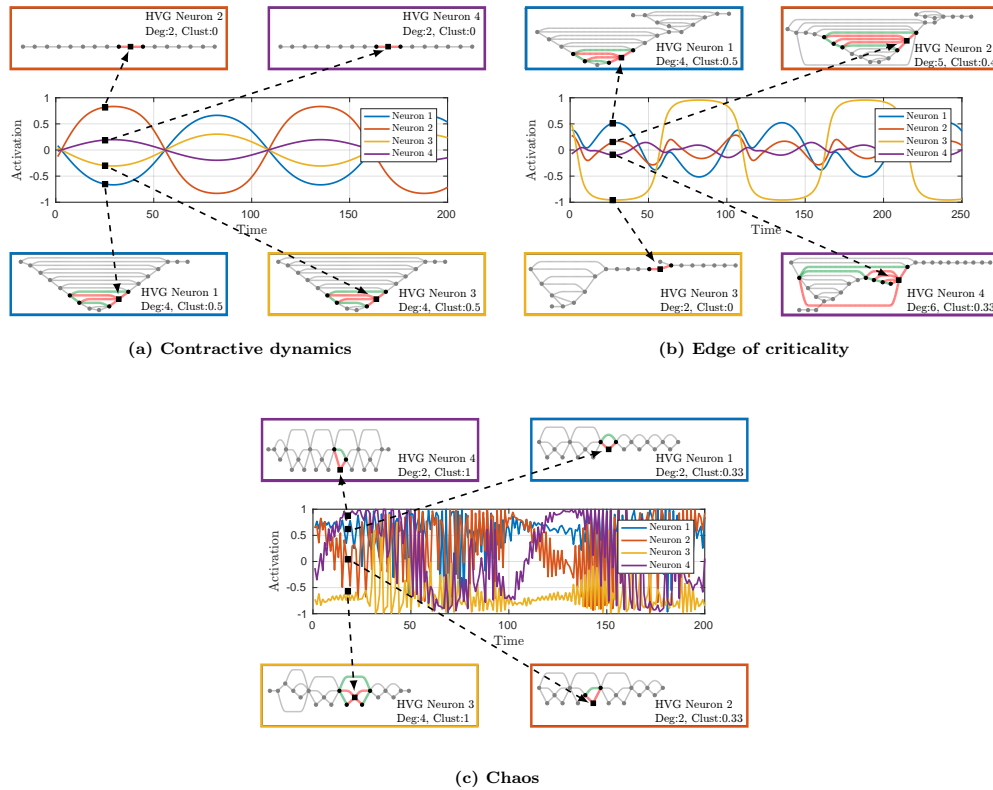


Figure 1. Illustration of the notion of heterogeneity in the instantaneous graph-based state. From each time series, we visualize only a portion of its visibility graph and consider a specific time step, marked by black squares in the figure. In the HVGs, we highlight in red the edges connecting each vertex that corresponds to the selected time step. For the clustering coefficient, instead, one has to consider also edges highlighted in green. The non-local nature of RNN graph-based state is evident from such representations, since vertices can be connected to other vertices that are associated to time instants far away along the sequence.

configured with a contractive dynamic, neuron activations weakly depend on previous RNN states and they are all very similar to the driving input signal. This results in a lack of diversity among activations. Accordingly, the corresponding HVGs in the

multiplex contain vertices with similar properties, e.g., similar degree and clustering coefficient. When a RNN approaches the edge of criticality, the activities of the neurons show a high degree of dependence from previous internal states, which encode information of past inputs and internal structure of neuron connections. These latter are constructed to be as different as possible and hence the diversity in the activations is obtained. As we can see in Fig. 1, on the edge of criticality the activations have different frequencies and their phases are shifted. Such a heterogeneity of the RNN instantaneous state is captured by the vertex properties in the multiplex. Finally, the RNN enters a chaotic regime if pushed beyond this edge. In this case, activations become noise-like and disordered oscillations generate HVG vertex properties that are very different from previous configurations. However, the presence of well-defined patterns characterizing different time series disappears, hence heterogeneity is again lost. The lack of variety is also highlighted by recurrence of same motifs in the corresponding HVGs.

By referring to the schema in Fig. 2, we observe that, at given time t , the RNN state is represented by those vertices in the multiplex tagged with the same label across the layers; for example, the ones in red describe the instantaneous state of the RNN at time step t_4 . According to the procedure described in the methodological section, a vector of vertex properties $\Phi^*[t_4]$ is computed for this set of vertices. Then, we estimate the distribution $p(\Phi^*[t_4])$ and the entropy $H_4^* = H(p(\Phi^*[t_4]))$. The procedure is repeated for each time step to compute \bar{H}^* , which is used to characterize the current configuration of the RNN hyperparameters. The average entropy depends on the specific vertex property chosen for the analysis, namely vertex degree, clustering coefficient, betweenness and closeness centrality (see Methods). These lead to four different quantities \bar{H}^{DG} , \bar{H}^{CL} , \bar{H}^{BC} , and \bar{H}^{CC} . We identify the regions in the hyperparameter space where these entropies are maximized as the edge of criticality for the RNN fed with a specific input signal. Accordingly, this information can be used to derive optimal configurations in an unsupervised way.

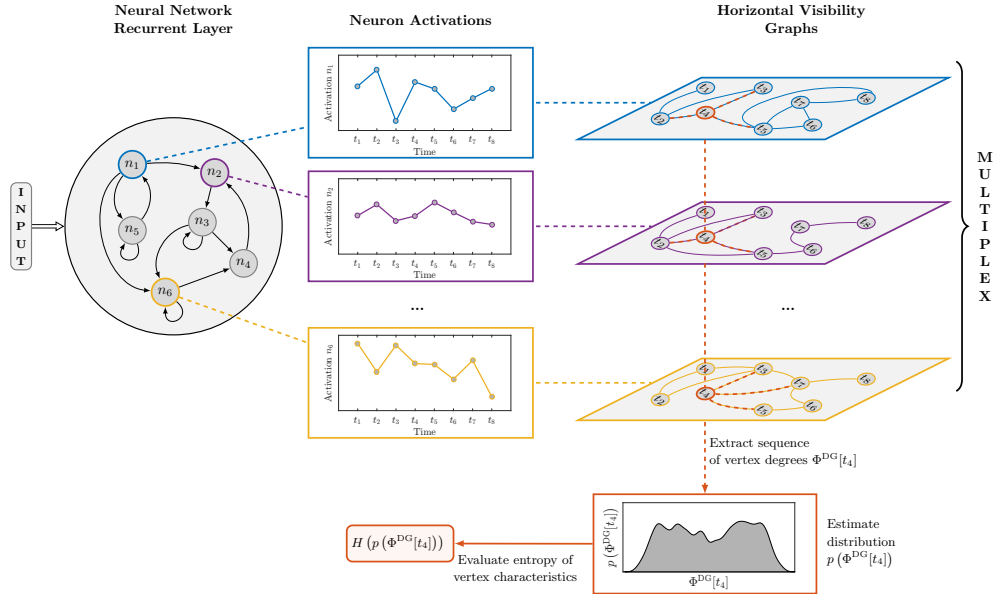


Figure 2. High-level schema of the proposed methodology. Activity in a RNN driven by some input signal is analyzed through a multivariate time series of neuron activations. We map such time series with a multiplex formed by HVGs on the layers. Hence, we get rid of problems related to stationarity and dependence in the activations. With such a representation, the state of the RNN is defined through graph-theoretical tools, which allow to include non-local (in time) information in the RNN instantaneous state. For instance at time instant t_4 , instead of the original activations, we consider a vertex property (e.g., vertex degrees $\Phi^{DG}[t_4]$) of the HVG to represent the RNN state. The instantaneous state is eventually characterized by a measure of heterogeneity of such values – here entropy is taken into account.

In our experiments, we consider several prediction tasks on an ESN and, for each of them, we set the forecast step $\tau_f > 0$ to be the smallest time-lag that guarantees the measurements in the interval to be uncorrelated (e.g., the first zero in the autocorrelation function of the input signal). To evaluate prediction error, we adopt the Normalized Root Mean Squared Error, $\text{NRMSE} = \sqrt{\langle \|\mathbf{y}[t] - \hat{\mathbf{y}}[t]\|^2 \rangle / \langle \|\hat{\mathbf{y}}[t] - \langle \mathbf{y}[t] \rangle\|^2 \rangle}$, where $\hat{\mathbf{y}}[t]$ is the ESN prediction and $\mathbf{y}[t]$ the desired/teacher output. Prediction accuracy (γ) is defined as $\gamma = \max\{1 - \text{NRMSE}, 0\}$.

In the following we describe five different widely used benchmarks. We also consider a time series relative to real-world data.

Sinusoidal input: this task consists in predicting a sinusoidal signal $y(t) = \sin(\psi t)$ with a forecast step $\tau_f = \frac{2\pi}{\psi}$.

Mackey-Glass time-series: the Mackey-Glass (MG) system is commonly used as benchmark in chaotic time series prediction. The input signal is generated from the MG time-delay differential equation

$$\frac{dx}{dt} = \frac{\alpha x(t - \tau_{\text{MG}})}{1 + x(t - \tau_{\text{MG}})^{10}} - \beta x(t).$$

We adopt the standard parameters $\tau_{\text{MG}} = 17, \alpha = 0.2, \beta = 0.1$, initial condition $x(0) = 1.2$, and integration step equal to 0.1. The forecast step here is $\tau_f = 6$.

Multiple superimposed oscillator: prediction of superimposed sinusoidal waves with fractional frequencies is a hard forecast exercise, since the wavelength can be extremely long. Here, we consider the multiple superimposed oscillator (MSO) studied in³⁷ and defined as

$$y(t) = \sin(0.2t) + \sin(0.311t) + \sin(0.42t).$$

For this task, we set $\tau_f = 16$.

NARMA: the Non-Linear Auto-Regressive Moving Average (NARMA) task, originally proposed in³⁸, consists in modeling the output of the following r -order system:

$$y[t+1] = 0.3y[t] + 0.05y[t] \left(\sum_{i=0}^r y[t-i] \right) + 1.5x[t-r]x[t] + 0.1.$$

$x[t]$ is a uniform random noise in $[0, 1]$, and the model is trained to reproduce $y[t+1]$. The NARMA task is known to require a memory of at least r past time-steps, since the output is determined by this input and outputs from the last r time-steps. For this prediction task we set $r = 20$ and $\tau_f = 15$.

Polynomial task: in this test, firstly introduced in³⁹, the ESN is fed with uniform noise in $[-1, 1]$ and is trained to produce an output according to

$$y[t] = \sum_{i=0}^p \sum_{j=0}^{p-i} c_{i,j} x^i[t] x^j[t-d] \quad \text{s.t. } i+j \leq p,$$

where $c_{i,j}$ is a uniformly distributed number drawn from $[0, 1]$. Difficulty of prediction can be controlled by varying the degree p of the polynomial and the time delay d . In the experiments, we set $p = 7, d = 10$ and $\tau_f = d$.

Telephone call load time series: as last test, we consider a real-world dataset relative to the load of phone calls registered over a mobile network. The dataset consists of 6 time series: number and volume (in minutes) of incoming calls, number and volume (in minutes) of outgoing calls, day and hour when the telephone activity was registered. Data come from the Orange telephone dataset, published in the Data for Development (D4D) challenge⁴⁰. D4D is a collection of call data records, containing anonymized events of Orange's mobile phone users in Ivory Coast, in a period spanning from December 1, 2011 to April 28, 2012. More detailed information are available on the related website¹. All 6 time series are fed into the ESN and we try to predict 6 hours ahead the volume (in minutes) of incoming calls – the profile of this latter time series is depicted in Fig. 3.

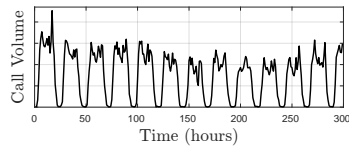


Figure 3. D4D dataset – load profile of incoming calls volume for the first 300 time intervals.

In each test, we evaluate, for different configurations of the hyperparameters ρ and ω_i , the correlation between average entropy of vertex properties in the multiplex and the prediction accuracy γ . Multiplexes are generated using both the binary and weighted version of HVG adjacency matrix. To appreciate the effectiveness of our methodology, we also estimate the correlations of γ with λ , the minimum singular value of the Jacobian of the reservoir (see Methods). Additionally, we consider the correlation of γ with the two layer-based measures IMI and AEO, described in Methods. Correlations are evaluated as follows. For each configuration ($\rho = k, \omega_i = j$), we have the prediction accuracy $\gamma_{k,j}$, the entropy $\bar{H}_{k,j}^{\text{DG}}$, and so on. The values assumed by these quantities by varying ρ and ω_i generate a two-dimensional manifold. The point-wise linear (Pearson) correlation between the manifolds relative to γ and to the other considered measures is the result we are interested in. The

¹<http://www.d4d.orange.com>

configurations of the hyperparameters examined are generated by varying ρ in $[0.5, 1.3]$ (20 different values) and ω_i in $[0.2, 0.9]$ (10 different values). A total of 200 configurations are evaluated. Due to stochastic nature of ESN initialization, for each configuration ($\rho = k, \omega_i = j$) we compute $\gamma_{k,j}$ and all other measures 15 different and independent times and then we compute correlations of their average values. We use a reservoir with $N_r = 100$ neurons and sparsity of the internal connectivity equal to 25%. The readout is trained by standard ridge regression with regularization parameter set to 0.05. Distributions of vertex properties are approximated by histograms with $b = 50$ bins.

Fig. 4 depicts the values assumed by γ and four graph-based measures in the case of the MSO prediction task. As it is possible to notice, there is high correlation between the (average) entropy of the vertex properties and the prediction accuracy. Since our approach is fully unsupervised, the proposed graph-based measures can approximate well the accuracy γ , regardless of the task learned by the readout (prediction, function approximation, reconstruction of past inputs, etc.).

In Tab. 2, we report the average correlation values and their statistical significance (expressed by the p -value) on all tasks. As we can see, the highest (and statistically significant) correlation is achieved by using one of the four average entropy measures of vertex properties. In particular, the measure based on vertex cluster coefficient distribution, \bar{H}^{CL} , achieves the best results over 5 of the 6 tasks. For what concerns the D4D time series, we observe that λ denotes high correlation with γ , but still lower than the one achieved by \bar{H}^{CL} . This demonstrates the effectiveness of the proposed methodology, also in the case of a real-world application. In SIN and MSO tasks, the graph-based quantifiers estimated on the weighted HVG achieve a higher degree of accuracy, with respect to the binary counterpart. In these cases, additional qualitative information relative to temporal and amplitude differences in the connected data allows to better represent the dynamics of the system. Finally, it is worth noting that IMI denotes high, yet negative correlation values on both MG and POLY tasks. In such cases, results are somewhat close to the ones achieved by means of the proposed measures based on average entropy of the vertex properties.

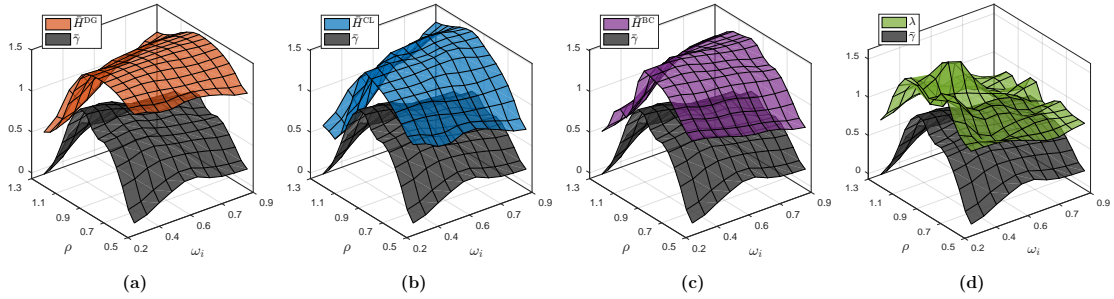


Figure 4. In each panel, the two-dimensional gray manifold represents the values of the prediction accuracy γ in MSO task, for different configurations of ρ and ω_i . The colored manifolds are the average entropy of the distributions of (a) vertex degree \bar{H}^{DG} , (b) clustering coefficient \bar{H}^{CL} , (c) betweenness centrality \bar{H}^{CC} . Finally, the manifold in (d) represents λ , which is computed from the ESN Jacobian. From the figure, it is possible to observe the correlation between the ESN performance, in terms of prediction accuracy, and the unsupervised measures derived from the multiplex representation of the ESN activity.

Test on memory capacity

As previously discussed, the edge of criticality has an impact also on memory capacity. In the following, we propose unsupervised, graph-based methods to identify the configurations where ESNs achieve large memory capacity.

According to the definition of MC (see Eq. 4), in order to evaluate the amount of memory in an ESN, different readouts are trained on the same reservoir, each one designed to reproduce a past version of the input signal at different time lags. Hence, MC is high if, by taking a linear combination of the states (recall from Methods that we are considering a linear readout), it is possible to reconstruct several delayed versions of the input. Given the input time series $\mathbf{x} = \{x[t]\}_{t=1}^{t_{\max}}$, an unsupervised method to quantify ESN memory consists in evaluating whether there exists a subset of neuron activations, \mathbf{H} , which carries the information contained in a past input sequence $\mathbf{x}_{a,b} = \{x[t - \tau_a], \dots, x[t - \tau_b]\}$, with $\tau_a > \tau_b$ and $\tau_a, \tau_b \in [1, t_{\max} - 1]$. The rationale behind the use of these unsupervised measures is that, a reservoir configured on the edge of criticality generates heterogeneous activations, each one depending on a combination of different sequences generated in the past by input signal and neuron activations. Therefore, if the reservoir dynamics are sufficiently rich, it is likely to find activations of at least one neuron that are related to a specific previous portion of the input signal. On the other hand, if internal dynamics are too contractive, neuron activations mostly depend only on recent inputs, resulting also in lack of diversity as discussed in the previous section. Finally, if the reservoir is operating in a chaotic regime, the high degree of divergence of the trajectories associated with neuron activations makes impossible the reconstruction of former input and state sequences.

Table 2. Correlations and related p -values (in brackets) of the proposed graph-based measures with accuracy γ in different prediction tasks, as ρ and ω change. We report the correlation of the manifolds generated by the values of γ with the manifolds relative to \bar{H}^{DG} , \bar{H}^{CL} , \bar{H}^{BC} , and \bar{H}^{CC} , which are the average entropy values of the distributions of vertex degree, clustering coefficient, betweenness and closeness centrality. Each measure is computed on both the binary (b) and weighted (w) versions of the HVG adjacency matrix (adj). We also report the correlations of γ with the manifolds relative to minimum singular value of the reservoir Jacobian over time (λ) and two multiplex-based measures AEO and IMI, presented in²¹. In each task, highest correlations with γ are highlighted in bold.

Task	adj	corr($\gamma, \bar{H}^{\text{DG}}$)	corr($\gamma, \bar{H}^{\text{CL}}$)	corr($\gamma, \bar{H}^{\text{BC}}$)	corr($\gamma, \bar{H}^{\text{CC}}$)	corr(γ, IMI)	corr(γ, AEO)	corr(γ, λ)
SIN	b	0.489 (0.006)	0.488 (0.006)	0.157 (0.333)	0.042 (0.797)	-0.091 (0.632)	-0.326 (0.040)	0.154 (0.343)
	w	0.662 (0.000)	0.705 (0.000)	0.694 (0.000)	-0.127 (0.436)			
MG	b	0.577 (0.000)	0.652 (0.000)	-0.37 (0.019)	0.438 (0.005)	-0.617 (0.000)	0.414 (0.008)	-0.19 (0.239)
	w	-0.138 (0.396)	0.330 (0.038)	0.046 (0.777)	0.564 (0.000)			
MSO	b	-0.215 (0.183)	-0.206 (0.201)	0.427 (0.006)	0.333 (0.036)	-0.238 (0.139)	-0.312 (0.05)	0.571 (0.000)
	w	0.628 (0.000)	0.810 (0.000)	0.820 (0.000)	-0.246 (0.125)			
NARMA	b	0.511 (0.001)	0.514 (0.001)	-0.332 (0.037)	-0.473 (0.002)	-0.543 (0.000)	-0.472 (0.002)	0.399 (0.011)
	w	-0.373 (0.018)	-0.185 (0.254)	-0.420 (0.007)	-0.376 (0.017)			
POLY	b	0.755 (0.000)	0.765 (0.000)	-0.393 (0.012)	-0.306 (0.055)	-0.745 (0.000)	0.440 (0.005)	-0.557 (0.000)
	w	-0.133 (0.412)	-0.113 (0.487)	0.47 (0.002)	-0.171 (0.291)			
D4D	b	0.632 (0.000)	0.677 (0.000)	-0.233 (0.104)	0.061 (0.676)	-0.611 (0.000)	0.168 (0.243)	0.670 (0.000)
	w	-0.455 (0.001)	-0.604 (0.000)	0.189 (0.188)	-0.409 (0.003)			

By referring to the measures defined in Methods, the most straightforward approach consists in evaluating the similarity $\delta^{\text{TS}}(\mathbf{x}_{a,b}, \mathbf{H})$ directly on the time series. As an alternative, here we propose a graph-based method to analyze the information content that \mathbf{H} carries about $\mathbf{x}_{a,b}$. In particular, we generate the HVGs $G_{\mathbf{x}}, G_1, \dots, G_{N_r}$, relative to delayed input $\mathbf{x}_{a,b}$ and to neuron activations, respectively, and successively evaluate their similarities by means of δ^{DG} and δ^{AND} . We consider the three different similarity measures κ^{PC} , κ^{SC} , and κ^{MI} to compute δ^{TS} and δ^{DG} . Fig. 5 provides an illustration explaining the proposed method and how δ^{DG} is computed.

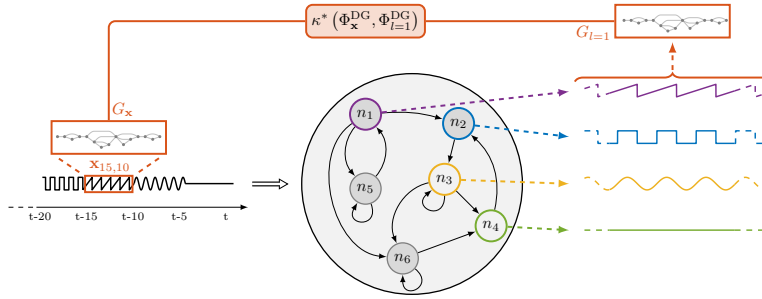


Figure 5. We extract a subsequence from the history of the input signal, for example $\mathbf{x}_{15,10}$, and compute the associated HVG $G_{\mathbf{x}}$. We repeat the procedure for each neuron activation, ending up with the HVGs $G_{l=1}, \dots, G_{l=N_r}$. For each HVG, we compute the sequence of vertex degrees and evaluate the similarities $\kappa^*(\Phi_{\mathbf{x}}^{\text{DG}}, \Phi_{l=1}^{\text{DG}})$ for $l = 1, \dots, N_r$. The largest of this similarity values is the value of δ^{DG} . In this example, the activation generated by neuron n_1 is clearly the most related one with the input sequence $\mathbf{x}_{15,10}$ and therefore it is the one that determines the value of δ^{DG} .

The performed experiment consists in generating 100 different random reservoirs, each one characterized by an increasing value of spectral radius ρ in the $[0.1, 2]$ interval. As ρ varies, we evaluate the MC by training four different readouts to reproduce four time-lagged versions of input signal $\mathbf{x}_{10,5}, \dots, \mathbf{x}_{25,20}$. Then, from each reservoir, we evaluate the similarities δ^{TS} , δ^{DG} , and δ^{AND} , which are high if there exists at least one series of activations that is similar to the considered past input sequence. This is evaluated according to the measure κ^* taken into account. Even if some neurons retain dynamics of previous input sequences, the reservoir introduces shifts in phase and amplitude of the input signal. To filter out these differences, in this memory test we only consider HVGs defined by binary adjacency matrices, which do not account for differences in amplitude of the connected values. To evaluate the effectiveness of the proposed unsupervised memory measures, we compute the correlation between the supervised MC and δ^{TS} , δ^{DG} , δ^{AND} , as ρ varies. Note that we only monitor the effect of ρ on the

dynamics, since it is the hyperparameter that mostly affects the amount of memory³⁰. We kept the input scaling fixed, $\omega_i = 0.7$, while the remaining hyperparameters are configured as in the previous experiment. As before, we repeated each experiment 15 times with different and independent random initializations. In Tab. 3, we show the mean correlation values, along with standard deviations, between MC and the proposed unsupervised measures of memory.

Table 3. Mean correlations and standard deviations of MC with the unsupervised memory quantifiers δ^{TS} , δ^{DG} , and δ^{AND} . We consider 4 different sequences of past inputs $\mathbf{x}_{10,5}, \dots, \mathbf{x}_{25,20}$. Values for each measure are computed as the spectral radius ρ of ESNs reservoir varies from 0.1 to 2. To compute δ^{TS} and δ^{DG} , we consider three different similarities: Pearson correlation κ^{PC} , Spearman correlation κ^{SC} , and mutual information κ^{MI} . Best results for each input sequence are reported in bold.

Input sequence	$\text{corr}(\delta^{\text{TS}}, \text{MC})$			$\text{corr}(\delta^{\text{DG}}, \text{MC})$			$\text{corr}(\delta^{\text{AND}}, \text{MC})$
	κ^{PC}	κ^{SC}	κ^{MI}	κ^{PC}	κ^{SC}	κ^{MI}	
$\mathbf{x}_{10,5}$	0.608 ± 0.094	0.594 ± 0.096	0.235 ± 0.054	0.682 ± 0.036	0.693 ± 0.029	0.607 ± 0.057	0.771 ± 0.034
$\mathbf{x}_{15,10}$	0.542 ± 0.042	0.546 ± 0.048	0.484 ± 0.047	0.547 ± 0.052	0.645 ± 0.038	0.343 ± 0.056	0.518 ± 0.043
$\mathbf{x}_{20,15}$	0.556 ± 0.068	0.550 ± 0.065	0.387 ± 0.038	0.776 ± 0.040	0.818 ± 0.046	0.182 ± 0.068	0.665 ± 0.075
$\mathbf{x}_{25,20}$	0.607 ± 0.043	0.603 ± 0.050	0.431 ± 0.066	0.811 ± 0.015	0.828 ± 0.019	0.501 ± 0.052	0.468 ± 0.147

From the table, we observe that the best level of agreement with MC is achieved by the measures derived from the HVGs. In particular, δ^{DG} configured with the Spearman rank κ^{SC} is always highly correlated with MC and, in three of the four delayed input sequences taken into account, is the one which obtains the best result. In each setup, δ^{DG} performs better when configured with κ^{SC} rather than κ^{PC} . Instead, results obtained considering κ^{MI} are significantly worse in all cases. δ^{AND} achieves the best results only for the first time lag taken into account, although the agreement with MC is lower in the remaining cases. Interestingly, several measures show a high degree of correlation with MC as the size of delay increases. δ^{TS} , the unsupervised measure computed directly on the input and neuron activations time series, shows positive correlations with MC, but the level of agreement is always lower than other graph-based measures. For δ^{TS} , the setting with κ^{PC} works better than κ^{SC} . Finally, also in this case by using κ^{MI} we obtain the worst performance. In Fig. 6, we show an example of the values of MC, δ^{TS} (configured with κ^{PC}), δ^{DG} (configured with κ^{SC}), and δ^{AND} , as ρ is varied within the chosen interval.

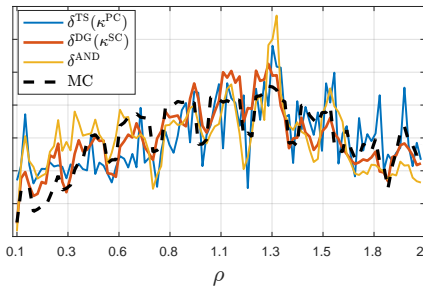


Figure 6. Values generated by supervised and unsupervised memory measures, when input sequence $\mathbf{x}_{20,15}$ is taken into account. In this case, we can see that the agreement of MC with δ^{DG} (using κ^{SC}) is higher than δ^{TS} (using κ^{PC}) and δ^{AND} , as ρ varies in $[0.1, 2]$.

Discussion

Experimental results show satisfactory correlations for average entropy of vertex properties with respect to prediction accuracy. Moreover, the two unsupervised graph-based memory measures that we proposed correlate well with the supervised measure of memory capacity. We first discuss the results of the prediction accuracy test, where we analyzed topological properties of vertices in the multiplex, representing the ESN instantaneous state. We observed a remarkable correlation between γ and the average entropy of the clustering coefficient distribution \bar{H}^{CL} , which describes well the heterogeneity of the activations. To explain this result, it is necessary to elaborate on the clustering coefficient properties $\text{CL}(\cdot)$. In the HVG literature, $\text{CL}(\cdot)$ has been analyzed in⁴¹, where authors discuss its behavior as the Hurst exponent characterizing the time series varies. Also, in²² authors provide an upperbound ($\text{CL}(v) \in [0, 2/\text{DG}(v)]$) for HVGs derived from random time series. In the following, we provide an in-depth interpretation of the results by accounting for geometrical properties of clustering coefficient.

In a HVG, $\text{CL}(v)$ measures the inter-visibility among neighbors of v . For convex functions, it is possible to connect any two points with a straight line. This feature is also (partially) captured by the HVG. If v is contained in a convex part of the related

time series, there is a high degree of intervisibility among the neighbor vertices to which v is connected, hence $CL(v)$ is high. Additionally, moving along the same convex part of the time series results only in minor changes of the clustering coefficient in the associated HVG vertices. If, instead, v is a local maximum of a concave part, it is connected to points belonging to two different basins, which do not have reciprocal visibility. In this case, $CL(v)$ is low and its value rapidly changes as one moves away from the maximum. This results in great losses of visual information. Hence, large values of $CL(\cdot)$ indicate the presence of dominating convexities, while low values characterize concavities⁴². Accordingly, $CL(\cdot)$ can be used to measure the length of a convex (concave) part of the time series and how fast the convexity is changing, which is a measure of the fluctuations in the time series⁴³. In a regime characterized by contractive dynamics, convexity changes uniformly in different neuron activations and this results in a low entropy value of clustering coefficient distribution among vertices in different layers. On the edge of criticality, instead, convex and concave parts in the time series of activations are characterized by heterogeneous lengths and they change at different rates. This corresponds to a high degree of clustering coefficient diversity of the same HVG vertex, replicated at different layers in the multiplex. Finally, in the chaotic regime, all time series fluctuate very rapidly and their convexity changes every few time steps. In this case, the lengths of convex and concave parts are always very short in each time series of activations and hence the desired heterogeneity is again lost.

For what concerns experiments on memory, the best overall results in terms of agreement with the supervised MC are achieved by the graph-based measure δ^{DG} . As previously discussed, such measure evaluates the maximum similarity between the sequence of vertex degrees on the input HVG G_x and the HVG G_l of neuron activations. This measure is closely related with the degree distribution $P(k)$, whose importance is known in the HVG literature²². For example, it has been shown that for time series generated from an i.i.d. process, $P(k)$ follows $P(k) = (1/3)(2/3)^{k-2}$ and the mean degree is $\langle k \rangle = 4$. As the correlations in the time series increase, the i.i.d. assumption is lost and $P(k)$ decays faster. Furthermore, vertex degrees are key parameters to describe dynamic processes on the graph, such as synchronization of coupled oscillators, percolation, epidemic spreading, and linear stability of equilibrium in networked coupled systems⁴⁴. Their role has been studied also in the HVG framework⁴⁵. HVGs have been studied in the context of time series related to processes with power-law correlations⁴¹. In our case, the time series of neuron activations have short-term correlations and increments in the correlation coefficients can have opposite signs at consecutive time lags. For these cases, we are not aware of any previous study in terms of HVGs.

In networks which are inherently degree disassortative, the range of degree values increases with network size, with a consequent decrease of the assortativity value⁴⁶. In such networks, the Spearman rank correlation provides a more suitable choice with respect to calculating degree-degree Pearson correlations. It is important to notice that the rank is computed through a non-linear rescaling, which is data dependent. The information on the actual values of the data is discarded as only its inherent ordering (rank) is preserved. We argue that HVGs convey the same type of information captured by the Spearman correlation. Hence, the latter should be preferred to Pearson correlation to characterize the characteristics of the vertices and related topological properties in HVGs. This fact justifies the higher agreement with memory capacity achieved by means of δ^{DG} when configured with κ^{SC} , which accounts for Spearman correlations between sequences of vertex degrees in the HVGs related to input signal and reservoir neuron activations.

By modeling RNN dynamics through a multiplex, we connected two seemingly different research fields and fostered multidisciplinary research. By converting a temporal problem into a structural one, we handled temporal dependencies introduced by RNNs, overcoming the limitations of statistical approaches that require independence of samples. Through several experiments, we provided empirical evidence that our methodology achieves performance higher than other unsupervised approaches and comparable to cross-validation techniques. To our knowledge, this is the first time RNNs are studied within the framework of multiplex networks. While this paper is primarily focused on network structures in machine learning context, our results might suggest new ideas for theoretical understanding of recurrent structures in biological neural networks, as well as memory properties in other systems with similar dynamics, like opinion dynamics in social networks.

Author contributions

FMB and LL designed methods and wrote the paper. FMB performed experiments. CA and RJ revised the paper. All authors read and approved the final manuscript.

Competing financial interests

The authors declare that there is no conflict of interest.

References

1. Barzel, B. & Barabási, A-L. Universality in network dynamics. *Nature Physics* **9**, 673–681 (2013).

2. Maass, W., Joshi, P. & Sontag, E. D. Computational aspects of feedback in neural circuits. *PLoS Computational Biology* **3**, e165 (2007).
3. Reinhart, R. F. & Steil, J. J. Regularization and stability in reservoir networks with output feedback. *Neurocomputing* **90**, 96–105 (2012).
4. Enel, P., Procyk, E., Quilodran, R. & Dominey, P. F. Reservoir computing properties of neural dynamics in prefrontal cortex. *PLoS Computational Biology* **12**, e1004967 (2016).
5. Hammer, B., Micheli, A., Sperduti, A. & Strickert, M. Recursive self-organizing network models. *Neural Networks* **17**, 1061–1085 (2004).
6. Charles, A., Yin, D. & Rozell, C. Distributed sequence memory of multidimensional inputs in recurrent networks. *arXiv preprint arXiv:1605.08346* (2016).
7. Tiño, P. & Rodan, A. Short term memory in input-driven linear dynamical systems. *Neurocomputing* **112**, 58–63 (2013).
8. Bianchi, F., Livi, L. & Alippi, C. Investigating echo state networks dynamics by means of recurrence analysis. *arXiv preprint arXiv:1601.07381* (2016). Under review at IEEE Transactions on Neural Networks and Learning Systems.
9. Sussillo, D. & Barak, O. Opening the black box: Low-dimensional dynamics in high-dimensional recurrent neural networks. *Neural Computation* **25**, 626–649 (2013).
10. Verstraeten, D. & Schrauwen, B. On the quantification of dynamics in reservoir computing. In *Artificial Neural Networks—ICANN 2009*, 985–994 (Springer Berlin Heidelberg, 2009).
11. Boedecker, J., Obst, O., Lizier, J. T., Mayer, N. M. & Asada, M. Information processing in echo state networks at the edge of chaos. *Theory in Biosciences* **131**, 205–213 (2012).
12. Livi, L., Bianchi, F. & Alippi, C. Determination of the edge of criticality in echo state networks through Fisher information maximization. *arXiv preprint arXiv:1603.03685* (2016). Under review at IEEE Transactions on Neural Networks and Learning Systems.
13. Legenstein, R. & Maass, W. What makes a dynamical system computationally powerful? In Haykin, S., Principe, J., Sejnowski & McWhirter (eds.) *New Directions in Statistical Signal Processing: From Systems to Brain*, 127–154 (MIT Press, Cambridge, 2007).
14. Mayer, N. M. Input-anticipating critical reservoirs show power law forgetting of unexpected input events. *Neural Computation* **27**, 1102–1119 (2015).
15. Leisch, F., Trapletti, A. & Hornik, K. Stationarity and stability of autoregressive neural network processes. In Kearns, M. J., Solla, S. A. & Cohn, D. A. (eds.) *Advances in Neural Information Processing Systems 11*, 267–273 (MIT Press, 1999).
16. Lee, K.-M., Min, B. & Goh, K.-I. Towards real-world complexity: an introduction to multiplex networks. *The European Physical Journal B* **88**, 1–20 (2015).
17. Boccaletti, S. *et al.* The structure and dynamics of multilayer networks. *Physics Reports* **544**, 1–122 (2014).
18. Menichetti, G., Remondini, D., Panzarasa, P., Mondragón, R. J. & Bianconi, G. Weighted multiplex networks. *PloS ONE* **9**, e97857 (2014).
19. Kivelä, M. *et al.* Multilayer networks. *Journal of Complex Networks* **2**, 203–271 (2014).
20. De Domenico, M. *et al.* Mathematical formulation of multilayer networks. *Physical Review X* **3**, 041022 (2013).
21. Lacasa, L., Nicosia, V. & Latora, V. Network structure of multivariate time series. *Scientific Reports* **5** (2015).
22. Luque, B., Lacasa, L., Ballesteros, F. & Luque, J. Horizontal visibility graphs: Exact results for random time series. *Physical Review E* **80**, 046103 (2009).
23. Luque, B., Lacasa, L., Ballesteros, F. J. & Robledo, A. Analytical properties of horizontal visibility graphs in the Feigenbaum scenario. *Chaos: An Interdisciplinary Journal of Nonlinear Science* **22**, 013109 (2012).
24. Luque, B., Lacasa, L., Ballesteros, F. J. & Robledo, A. Feigenbaum graphs: A complex network perspective of chaos. *PLoS One* **6**, e22411 (2011).
25. Luque, B., Cordero-Gracia, M., Gómez, M. & Robledo, A. Quasiperiodic graphs at the onset of chaos. *Physical Review E* **88**, 062918 (2013).
26. Lacasa, L. & Toral, R. Description of stochastic and chaotic series using visibility graphs. *Physical Review E* **82**, 036120 (2010).

27. Ravetti, M. G., Carpi, L. C., Gonçalves, B. A., Frery, A. C. & Rosso, O. A. Distinguishing noise from chaos: Objective versus subjective criteria using horizontal visibility graph. *PLoS ONE* **9**, e108004 (2014).
28. Lukoševičius, M. & Jaeger, H. Reservoir computing approaches to recurrent neural network training. *Computer Science Review* **3**, 127–149 (2009).
29. Grigoryeva, L., Henriques, J., Larger, L. & Ortega, J.-P. Optimal nonlinear information processing capacity in delay-based reservoir computers. *Scientific Reports* **5** (2015).
30. Ozturk, M. C., Xu, D. & Príncipe, J. C. Analysis and design of echo state networks. *Neural Computation* **19**, 111–138 (2007).
31. Hermans, M. & Schrauwen, B. Recurrent kernel machines: Computing with infinite echo state networks. *Neural Computation* **24**, 104–133 (2012).
32. Manjunath, G. & Jaeger, H. Echo state property linked to an input: Exploring a fundamental characteristic of recurrent neural networks. *Neural Computation* **25**, 671–696 (2013).
33. Saramäki, J., Kivelä, M., Onnela, J.-P., Kaski, K. & Kertesz, J. Generalizations of the clustering coefficient to weighted complex networks. *Physical Review E* **75**, 027105 (2007).
34. Boccaletti, S., Latora, V., Moreno, Y., Chavez, M. & Hwang, D. Complex networks: Structure and dynamics. *Physics Reports* **424**, 175–308 (2006).
35. Lopez-Fernandez, L., Robles, G. & Gonzalez-Barahona, J. M. Applying social network analysis to the information in CVS repositories. In *Proceedings of the International Workshop on Mining Software Repositories*, 101–105 (Edinburgh, UK, 2004).
36. Bertschinger, N. & Natschläger, T. Real-time computation at the edge of chaos in recurrent neural networks. *Neural Computation* **16**, 1413–1436 (2004).
37. Jaeger, H. & Haas, H. Harnessing nonlinearity: Predicting chaotic systems and saving energy in wireless communication. *science* **304**, 78–80 (2004).
38. Jaeger, H. Adaptive nonlinear system identification with echo state networks. In *Advances in Neural Information Processing Systems*, 593–600 (MIT Press, 2002).
39. Butcher, J., Verstraeten, D., Schrauwen, B., Day, C. & Haycock, P. Reservoir computing and extreme learning machines for non-linear time-series data analysis. *Neural Networks* **38**, 76 – 89 (2013).
40. Blondel, V. D. *et al.* Data for Development: the D4D Challenge on Mobile Phone Data. *ArXiv preprint arXiv:1210.0137* (2012).
41. Xie, W.-J. & Zhou, W.-X. Horizontal visibility graphs transformed from fractional Brownian motions: Topological properties versus the Hurst index. *Physica A: Statistical Mechanics and its Applications* **390**, 3592–3601 (2011).
42. Costa, L. d. F., Rodrigues, F. A., Traverso, G. & Villas Boas, P. R. Characterization of complex networks: A survey of measurements. *Advances in Physics* **56**, 167–242 (2007).
43. Turner, A., Doxa, M., O’Sullivan, D. & Penn, A. From isovists to visibility graphs: A methodology for the analysis of architectural space. *Environment and Planning B: Planning and Design* **28**, 103–121 (2001).
44. Restrepo, J. G., Ott, E. & Hunt, B. R. Approximating the largest eigenvalue of network adjacency matrices. *Physical Review E* **76**, 056119 (2007).
45. Fioriti, V., Tofani, A. & Di Pietro, A. Discriminating chaotic time series with visibility graph eigenvalues. *Complex Systems* **21** (2012).
46. Newman, M. E. J. Assortative mixing in networks. *Physical Review Letters* **89**, 208701 (2002).